Single-molecule force spectroscopy reveals structural differences of heparan sulfate chains during binding to vitronectin

Katarzyna Herman,[1] Joanna Zemła,[2] Arkadiusz Ptak,[1] and Małgorzata Lekka[2,*]

[1]*Institute of Physics, Faculty of Materials Engineering and Technical Physics, Poznan University of Technology, Piotrowo 3, PL-60965 Poznań, Poland*

[2]*Department of Biophysical Microstructures, Institute of Nuclear Physics, Polish Academy of Sciences, PL-31342 Kraków, Poland*

(Received 1 March 2021; revised 15 July 2021; accepted 22 July 2021; published 11 August 2021)

The syndecans represent an ongoing research field focused on their regulatory roles in normal and pathological conditions. The role of syndecans in cancer progression is well documented, implicating their importance in diagnosis and even proposing various potential cancer treatments. Thus, the characterization of the unbinding properties at the single-molecule level will appeal to their use as targets for therapeutics. In our study, syndecan-1 and syndecan-4 were measured during the interaction with the vitronectin HEP II binding site. Our findings show that syndecans are calcium ion dependent molecules that reveal distinct, unbinding properties indicating the alterations in the structure of heparan sulfate (HS) chains, possibly in the chain sequence or sulfation pattern. In this way, we suppose that HS chain affinity to extracellular matrix proteins may govern cancer invasion by altering the syndecans' ability to interact with cancer-related receptors present in the tumor microenvironment, thereby promoting the activation of various signaling cascades regulating tumor cell behavior.

DOI: 10.1103/PhysRevE.104.024409

I. INTRODUCTION

The syndecan (SDC) family is composed of two large (syndecan-1 and syndecan-3) and two small (syndecan-2 and syndecan-4) members [1]. These molecules, located in the plasma membrane, belong to transmembrane heparan sulfate type I proteoglycans that interact with numerous ligands such as growth factors [2] and enzymes [3], and extracellular matrix (ECM) proteins such as fibronectin, vitronectin, collagens, or laminins [4]. Various studies have already reported the significance of syndecan expression in the normal and disease-related functioning of cells [5–7]. Syndecan-1 (SDC-1) is primarily expressed in mesenchymal and epithelial cells, while syndecan-4 (SDC-4) is typical for a wide variety of cell types [8]. SDC-1 plays an essential role in regulating inflammation or chemokine gradient formation for transendothelial and transepithelial migrations of neutrophils [9,10]. SDC-4 is mainly associated with cellular adhesion and migration, where a synergistic link between integrins and syndecans has been postulated and partially demonstrated [11–13]. SDC-1 regulates $\alpha_V\beta_3$ or $\alpha_V\beta_5$ binding that affects, for example, the angiogenesis in cancer cells [14,15]. SDC-4 is frequently associated with β_1 and β_3 integrins in focal adhesions [16,17].

Syndecans are linear structures consisting of extracellular, transmembrane, and cytoplasmic parts [1,18]. The cytoplasmic part, specific for each syndecan, comprises two highly conserved domains flanking the variable region. Its typical role is linking syndecans to actin filaments, binding to PDZ (Post synaptic density protein, Drosophila disc large tumor suppressor, and Zonula occludens-1 protein) proteins, or promoting syndecan-specific signaling. The transmembrane domain participates in syndecan oligomerization. A conserved phenylalanine residue regulates the interactions among syndecans by promoting the formation of either homodimers or heterodimers [19]. The extracellular domain (ectodomain) contains cleavage sites for various metalloproteinases, releasing syndecan ectodomains in the ECM. The interactions of syndecans with integrins involves either an NXIP motif (amino acids (AA): N- Asp; X - any AA; I - Ie; P - Pro; SDC-4, [20]) or a synstatin part (SDC-1, [21]). Ectodomains bear covalently attached glycosaminoglycans (GAGs) that, depending on the member type of the syndecan family, are composed of chondroitin (CS) and/or heparan (HS) sulfate chains. SDC-1 contains both CS and HS, while SDC-4 possesses only three HS chains (a single model has been built only for a syndecan ectodomain with three HS chains, but no experimental data confirm this structure [22]). The binding site of CS chains to syndecan-1 is membrane proximal, while the HS chains are located at sites at the N end of the SCD-1 protein core. In SCD-4, predominantly HS chains are bound at the N end, usually attached to serine or glycine sites on the syndecan core [1,23].

Unfortunately, despite the gathered extensive knowledge about syndecan involvement in integrin-mediated adhesion, the full details describing their participation are still lacking. Besides, the lack of complete structural data showing the entire ectodomains makes it challenging to predict how GAGs influence syndecan interaction with ECM proteins. Moreover, little is known about the dynamics of the GAG conformation changes accompanying the binding to ECM proteins, thus limiting the understanding of the syndecan role in various processes, such as signal transduction or integrin-mediated adhesion. We have recently shown that the expression of

*Malgorzata.Lekka@ifj.edu.pl

SDC-4 is significantly larger than the expression of SDC-1 in bladder cancer cells [5]. This supports the overall findings stating that the increase or decrease in the abundance of a specific member of the syndecan family has severe consequences affecting the invasion and progression of various cancers [5,24].

Since syndecans are involved in cell adhesion, their binding properties to extracellular matrix components are essential for understanding changes associated with distinct diseases. Several previous studies addressed the unbinding properties of syndecan-related complexes at the single-molecular level [5,12,25–27]. We quantified the unbinding properties between SDC-1 and SDC-4 and the corresponding monoclonal antibodies (Mabs) in our previous research. The results showed that these two specific syndecans interact differently. SDC-1 unbinds by passing over two energy barriers, inner and outer, while SDC-4 unbinds by crossing over only one energy barrier. Distinct unbinding pathways were attributed to structural differences of heparan and chondroitin chains. Moreover, the syndecan interaction with Mabs appeared to be calcium ion dependent. Although these results revealed family member dependent ways of interaction, in native conditions, syndecans interact with ECM in a synergistic way with integrins [11–13,27,28]. Syndecans participate synergistically in binding integrins to ECM proteins through di- or trimolecular complexes [12,27,28]. An example of the latter is Thy-1 [a glycosyl-phosphatidylinositol (GPI)-anchored adhesion protein] studies using force probes [12,27]. It has been shown that $\alpha_5\beta_1$, SDC-4, and Thy-1 cooperatively form a trimolecular complex. The binding of Thy-1 to the isolated integrin reveals a slip bond behavior, whereas similar binding to the integrin present on a cell surface manifests itself as a dynamic catch bond, being a reversible transition from slip to catch bonds. Such behavior has been proved to be linked with the presence of syndecan-4. Its role was associated with the change of bond mechanics resistance upon mechanical stimulation [12]. Further study shows that the role of SCD-4 is not repetitive, but oppositely it is dependent on the integrin type involved in the formation of trimolecular complex formation. In the system in which $\alpha_V\beta_3$ replaces $\alpha_5\beta_1$, SDC-4 stabilizes the interaction between the integrin and syndecan [27].

In our study, we employed an atomic force microscope (AFM) for single-molecule force spectroscopy (SMFS) [29,30] to study the binding of syndecans (SDC-1 and SCD-4) to vitronectin (VN, an ECM protein). The syndecans bind to the heparan-binding site (HEP II, 345–378 AA) located between two hemopexinlike domains at the C end of the vitronectin [31]. The later studies narrowed the binding sequence to 12 amino acids [Lys(Asp)347 to Gly358] located within the heparin initially defined binding domain [31–33]. All syndecans bind to the same HEP II binding site. Therefore, we ask ourselves what is the degree of specificity in such a recognition process. Our study hypothesizes that the unbinding process of single syndecan-vitronectin (SDC-VN) complexes is comparable for similar binding configurations, regardless of the syndecan type. Therefore, we expect to obtain similar thermodynamic and kinetic parameters from the force spectroscopy analysis for SDC-1 and SDC-4 complexes. To probe the unbinding properties of an individual SDC-VN complex, SDC-1 and SDC-4 were immobilized on a freshly cleaved mica surface while vitronectin was attached to the surface of silicon nitride cantilevers.

II. EXPERIMENTS: MATERIALS AND METHODS

A. Recombinant proteins

Vitronectin and syndecans were recombinant proteins purchased from R&D Systems. Syndecan-4 (SDC-4, $M_w = 24$ kDa; SDS PAGE, reducing conditions) consists of a signaling sequence (18 AA) attached to an extracellular domain (127 AA), a transmembrane region (25 AA), and a cytoplasmic tail (28 AA). Syndecan-1 (SDC-1, $M_w = 85$ kDa, SDS reducing conditions) consists of a signaling sequence (22 AA) attached to an extracellular domain (232 AA), a transmembrane region (21 AA), and a cytoplasmic tail (35 AA). An extracellular matrix protein—vitronectin (VN, Asp20-Leu478, 70–80 kDa SDS PAGE, reducing conditions)—consisted of a signaling peptide (19 AA) and a protein (459 AA). The amino-terminated end (130 AA) contains multiple binding sites, including an RGD sequence that binds to integrins, while the carboxyl-terminated end contains a heparin (HEP II) binding site. Its predominant structure is a monomer.

B. Monoclonal antibodies

The specific interactions involving syndecans were probed with monoclonal antibodies. They were MabSDC1 (A-6, Santa Cruz Biotechnology, Inc.), recognizing an amino acids sequence from 82 to 256 AA, an extracellular domain in SDC-1 of human origin, and MabSDC4 (5G9, Santa Cruz Biotechnology, Inc.), recognizing a sequence from 93 to 121 AA, an extracellular domain in SDC-4 of human origin. Solutions containing monoclonal antibodies were prepared by using phosphate-buffered saline (PBS, Sigma-Aldrich) buffer.

C. Mica surface modification

Syndecans (SCD-1 and SDC-4) were immobilized on an atomically flat, freshly cleaved muscovite mica surface (about 0.25 cm^2). First, the mica surface was silanized with 3-aminopropyl-triethoxysilane (1 ml, APTES, Signa-Aldrich, placed in a Petri dish) for 1.5 h in a desiccator. Afterwards, the silanized mica surface was activated with glutaraldehyde (2.5%) aqueous solution for 20 min. After glutaraldehyde activation, the mica surface was gently washed with PBS buffer. Syndecans were dissolved in the PBS buffer at the concentration of 0.2 μg/ml (molar concentrations were 2.4 nM and 8.3 nM for SDC-1 and SDC-4, respectively). A drop of such a solution was placed on the mica surface for 30 min. Afterwards, samples were thoroughly rinsed with PBS buffer to remove the excess of the unbound material.

D. Cantilever functionalization

To measure the unbinding force of SDC-1–VN or SDC-4–VN complexes, the surface of the silicon nitride cantilevers (PNP TR, NanoWorld) was coated with vitronectin (0.2 μg/ml dissolved in PBS buffer, the molar concentrations of 8.0 and 13.6 nM, respectively) for 25 min. Cantilevers were pretreated using an analogous procedure as for the mica surface

TABLE I. Theoretical accessibility of binding sites in the inhibition of the syndecans (0.2 μg/ml) by mixing them with the corresponding monoclonal antibodies (0.2 μg/ml).

Surface	Molar concentrations	Syndecan status
SDC-1 on mica	8.03 n*M*	100% of free SDC-1 are accessible
SDC-4 on mica	13.61 n*M*	100% of free SDC-4 are accessible
SCD-1–MabSDC1 (3.4:1) on mica	8.03:2.35 n*M*	71% of free SDC-1 are accessible
SDC-4–MabSDC4 (2:1) on mica	16.61:8.33 n*M*	50% of free SDC-4 are accessible

described above (1.5 h of silanization, 2.5% glutaraldehyde activation, PBS rinsing). After incubation with vitronectin, cantilevers were washed three times with the PBS buffer (2 min) and kept in the PBS buffer before measurements.

E. Single-molecule force spectroscopy

Measurements of the unbinding force were conducted using AFM head Force Robot (Bruker-JPK) working in automatized force spectroscopy mode (maximum Z range of 10 μm). The cantilever spring constant (PNP-TR, nominal value of 0.03 N/m, NanoWorld) was determined using the thermal fluctuation method [34]. All measurements were conducted in 50 m*M* Tris-buffered saline (TBS, Sigma-Aldrich) supplemented with 1 m*M* concentrations of Ca^{2+} and Mg^{2+} ions, $p\mathrm{H} = 7.6$. The use of the Force Robot head enabled us to carry out measurements in one run (4–5 days without a break, for setpoint at 500 pN) using one cantilever in a broad range of retraction velocities, from 0.1 to 19.0 μm/s (ten different velocities were chosen). The loading rate, calculated as a product of the effective spring constant (obtained from the slope of the force-displacement curve at the rupture event) and the retraction velocity, covers the range of 540–380 000 pN/s. The force curve acquisition process was carried out in cycles. Each cycle accounted for a 64×64 mesh of points localized on a 400 $\mu\mathrm{m}^2$ surface area, which delivered 4096 single force curves. The cycles were carried out pseudorandomly versus the retraction velocities to avoid the effect of tip wear in time. Each measurement cycle was acquired using the same cantilever. Measurements were repeated twice. All the force curves were analyzed with JPK SPM data processing software. There was no need to use a polymer linker because of the large size of molecules forming the studied complexes.

F. Assuring specificity of syndecan binding

To demonstrate the specificity of the interaction between SDC-VN complexes, the interaction was blocked in two ways. First, divalent ions were removed by adding 10 m*M* EDTA (Sigma-Aldrich) to the PBS solution. EDTA (ethylenediaminetetraacetic acid) binds and holds on to (chelates) metal ions; thus, it inhibits molecular interactions, in which metal ions participate [35]. We also applied Mabs against syndecans. In this case, the mica surface was functionalized with the solution containing a mixture of syndecan: MAbs (in a 1:1 ratio, concentrations of 0.2 μg/ml; molar concentrations were 2.4 and 8.3 n*M* for MabSDC1 and MabSDC4, respectively). Thus, on the mica surface, either individual syndecan molecules or SDC-VN complexes were present. The theoretical accessibility (calculated taking into account molar concentrations) was at the level of ∼71% and ∼50% for SDC-1–VN and SCD-4–VN complexes, respectively (Table I). This value represents the accessibility of the binding sites without considering the effect of molecule adsorption on the mica surface.

III. DYNAMIC FORCE SPECTROSCOPY—THEORETICAL MODELS

The dynamic force spectroscopy (DFS) spectra serve as a basis for the thermodynamic and kinetic characterization of the unbinding process, delivering information on the energy landscape of the interacting molecules. A few theoretical models describe a stochastic character of the escape process from a potential well such as Bell-Evans (BE, considers only the position of the energy barrier treated as a point, [36,37]), Dudko-Hummer-Szabo (DHS, considers the realistic shape of the energy barrier [38]), and Friddle-Noy–De Yoreo (FNDY, considers reversible bond formation, [39]). They can be applied to estimate the kinetic parameters of the unbinding process between single molecules. The BE model assumes that the applied external force lowers the height of the energy barrier. Evans and Ritchie have derived from the Bell formula the most probable unbinding force [36,37]:

$$F = \frac{k_B T}{x_\beta} \ln\left(\frac{r_f}{F_0 k_{\mathrm{off}}^0}\right), \tag{1}$$

where k_B is the Boltzmann constant, T is the absolute temperature, $F_0 = k_B T / x_\beta$, r_f is the loading rate, x_β is the distance between the maximum of an activation barrier and the bound state minimum (on the free-energy landscape), and k_{off}^0 is the force-free dissociation rate. By applying linear regression to the DFS data, one can easily extract the values of x_β and k_{off}^0; that is why the BE model has been widely applied to study specific interactions between molecules, including the receptor-ligand complexes [38–44]. This model has two main limitations: It ignores the rebinding processes and reduces all the information about the energy landscape profile (the interaction potential) to a single parameter—x_β. The DHS model goes beyond the BE by specifying the energy landscape profile and applying Kramer's diffusion theory [38]. In contrast to the BE model, additionally to x_β and k_{off}^0, it enables us to extract ΔG_β from the following expression for the most probable unbinding force:

$$F = \frac{\Delta G_\beta}{\nu x_\beta}\left\{1 - \left[\frac{k_B T}{\Delta G_\beta} \ln\left(\frac{k_{\mathrm{off}}^0 k_B T e^{\left(\frac{\Delta G_\beta}{k_B T}\right)}}{x_\beta r_f}\right)\right]^\nu\right\}, \tag{2}$$

where ΔG_β is the free energy of activation in the absence of external forces and the parameter ν is related to the shape of the free-energy potential. Its value of $2/3$, although specific

for the linear-cubic dependence, is appropriate for all smooth free-energy surfaces. The model has already been applied to analyze the interaction occurring in ligand-receptor binding [26,45] or self-assembled monolayers [46–48]. Both models, BE and DHS, ignore the possibility of reversible bond formation during force-induced unbinding experiments. This term has been introduced in the FNDY model that considers the rebinding contribution in the unbinding process described by Bell's formula [39]. The defined equilibrium force (F_{eq}) describes the force at which the unbinding passes from the near-equilibrium to the kinetic regime. It is related to the force at which the rates of dissociation and association of molecular complexes are in equilibrium:

$$F_{\mathrm{eq}} = \sqrt{2k_{\mathrm{eff}}\Delta G_{\mathrm{unb}}}. \tag{3}$$

Here, k_{eff} is the effective spring constant that considers the cantilever stiffness and the molecular complex, and ΔG_{unb} is the free energy of the unbound state relative to the bound one. The values of F_{eq} together with x_β and the dissociation rate at the equilibrium force, $k_{\mathrm{off}@F_{\mathrm{eq}}}$, describe the kinetics and strength of an intermolecular bond. The following equation approximates the mean unbinding force:

$$F \cong F_{\mathrm{eq}} + \frac{k_B T}{x_\beta}\ln\left(1 + e^{-\gamma}\frac{r_f}{\frac{k_B T}{x_\beta}k_{\mathrm{off}@F_{\mathrm{eq}}}}\right), \tag{4}$$

where $\gamma = 0.577$ is the Euler-Mascheroni constant. The main model application is the unfolding process of titin and the β-amyloid dimer rupture [45,49].

Fitting of the models to the data was performed using the ORIGINPRO 8.0 software using the NONLINEAR CURVE FIT analysis option. Before that, we built the fitting functions based on the theoretical models (BE, DHS, FNDY) using FITTING FUNCTION BUILDER. Our fitting procedure involves a variable set of initial values of the parameters to ensure that the optimal set of the parameters was found. It can be described as a local minimum in the meaningful part of the parameters space. The ORIGINPRO estimates the uncertainties of the derived parameters as standard errors according to the error propagation formula (for details, see [50]). In general, parameter uncertainties do not accurately reflect experimental errors and therefore should be treated only rather as indicators when comparing different fits and not as the estimation of absolute uncertainties of derived physical quantities.

IV. RESULTS AND DISCUSSION

A. Unbinding of single syndecan-VN complexes

To probe the unbinding properties of individual SDC-VN complexes (Fig. 1), SDC-1 and SDC-4 were immobilized on a freshly cleaved mica surface at the concentration of 0.2 μg/ml. Vitronectin was attached to the surface of silicon nitride cantilevers (0.2 μg/ml). The protocol, based on APTES and glutaraldehyde immobilization, has already been applied to study the interaction, for example, between ferritin and antiferritin [51], or carboxypeptidase Y (CaY) and concanavalin A (Con A) [52], or syndecans and antisyndecans [26].

Despite structural differences, syndecans interaction involves HS chains covalently attached at the N end in the syndecan core proteins. Thus, intuitively, such a binding

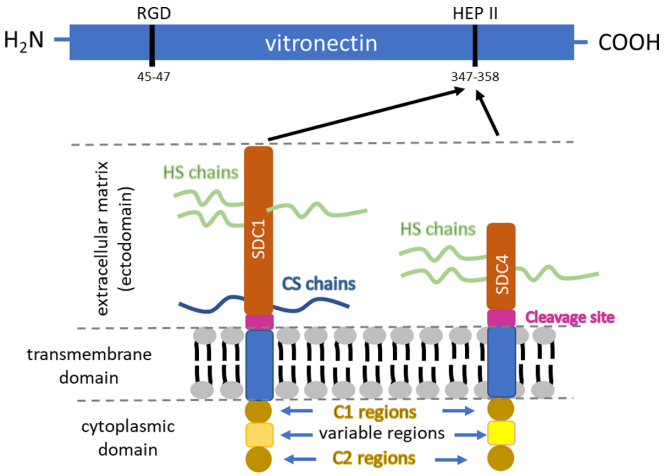

FIG. 1. Structure of syndecan-1 and syndecan-4 and the interaction with the HEP II binding site located at the C end of vitronectin.

seems to proceed similarly. Force curves were collected during the unbinding of the VN-modified AFM probe from the SDC-coated mica surface [inset in Fig. 2(a), simultaneously presenting an exemplary overlay of 20 force curves recorded for the SDC-1–VN complex].

Measurements were carried out in 50 mM TBS supplemented with 1 mM concentrations of Ca^{2+} and Mg^{2+}. An individual force curve represents the dependence between the cantilever vertical deflection (related to the unbinding force) and the tip-sample distance. Force curves [Fig. 2(b)], observed for SDC-VN interaction, were classified into the groups showing no adhesion or no specific interaction, a complex adhesion involving the multiple unbinding events, and single unbinding events attributed to a specific interaction of either SDC-1 or SDC-4 to vitronectin. We considered only a single molecule unbinding in the analysis, which accounted for about ~8% of all recorded force curves. After applying the same selection procedure for the data recorded in control experiments where a VN-modified cantilever interacts with the APTES-glutaraldehyde surface, the number of specific-like curves was below 1%.

B. Specificity of the syndecan-VN interaction

The interaction was blocked in various ways and quantified in terms of the unbinding probability to demonstrate the specificity of SDC-1–VN and SDC-4–VN unbinding (Fig. 3). This is the semiquantitative measure of how many specific unbinding events are observed at given experimental conditions, including retraction velocity. It is usually determined as a ratio between the number of specific unbinding events to the total number of force curves recorded.

In the condition of fully accessible binding sites, the probability of the unbinding events for the SDC-1–VN and SDC-4–VN was 7.5 ± 0.6% and 7.6 ± 0.8%, respectively. This is a much lower value than the theoretical accessibility (Table I), which can be explained by the strong effect of immobilization protocols on the binding site accessibility. Such a low value is desirable because, according to previous works, the unbinding probability of about 30% ensures an

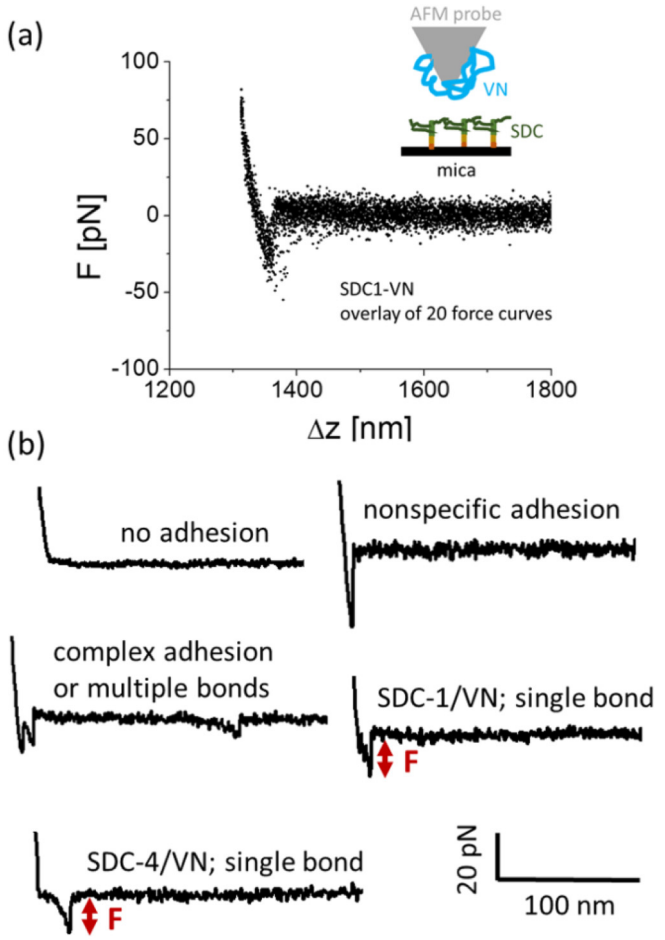

FIG. 2. (a) An exemplary overlay of 20 force curves recorded for the SDC-1–VN complex is presented. (b) Force curves showing no adhesion, nonspecific adhesion, or complex adhesion, including multiple unbinding events, were excluded from the analysis. Force curves showing the single-unbinding events characteristic for the rupture of SCD-1–VN and SDC-4–VN complexes.

83% chance that the measurement reflects a single receptor-ligand unbinding [40,53,54]. Thus, we may assume that the observed unbinding stems from a rupture of a single molecular complex. Having in mind the previously reported results [26], the unbinding measurements were conducted in 10 m*M* EDTA added to PBS. The results show a statistically significant drop in the unbinding probability to 3.9 ± 0.4% and 4.9 ± 0.3%, respectively. In the experiments when Mabs were used to block the SDC-VN interaction, syndecans were mixed with the corresponding Mabs at a 1:1 volumetric ratio, followed by the mixture deposition on the mica surface. The SMFS measurements showed a drop in the number of unbinding events to the level of 1.8 ± 0.2% (SCD-1–VN) and 2.3 ± 0.1% (SDC-4–VN), thus confirming that the selected force curves represent the specific recognition occurring between the studied complexes.

The obtained unbinding probabilities are smaller than those one could expect from the stoichiometric relations between the syndecans and the corresponding monoclonal antibodies. One could expect the unbinding probability at the level of 5.3% and 3.8% for SDC-1 and SDC-4, respectively. How-

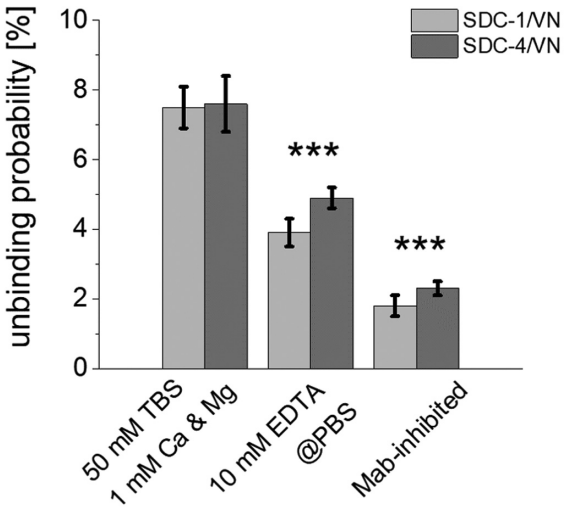

FIG. 3. The unbinding probability showing a decrease upon blocked SDC-VN interaction (data are mean ± standard deviation (SD), $^{***}p < 0.0001$). The means were calculated from all $n = 10$ repetitions (40 960 force curves) in TBS conditions and $n = 2$ repetitions (16 192 force curves for EDTA and Mab inhibition).

ever, these values indicate the ideal conditions in which all molecules deposited on a surface are accessible for antibody binding. The lower, experimentally derived values of the unbinding probabilities (i.e., 1.8% and 2.3% for SDC-1 and SDC-4, correspondingly, Table II) indicate that the number of syndecan molecules accessible for the antibody is far away from that calculated theoretically. However, the origin of this effect is not known. This might stem from the adsorption of syndecans on the mica surface, which is beyond the control for APTES-glutaradehyde functionalized surfaces. This effect seems to be more pronounced for longer SDC-1 than for shorter SDC-4.

A similar level of the unbinding probability suggests that in the syndecan-vitronectin interactions, all syndecans bind to heparan (HEP II) binding sites independently of their structure. In addition to results confirming the specificity of the interaction, we can also state that divalent ions are needed for the binding of syndecans to vitronectin. The Ca^{2+} and Mg^{2+} ions probably maintain HS chain conformation since they are covalently attached to the syndecan N end that protrudes significantly beyond the cell membrane. The more considerable drop in the unbinding probability obtained for the SDC-1–VN complex may also indicate differences in HS structures among the studied syndecans. These results agree with already reported data showing that divalent ions such as Mg^{2+}, together with heparan sulfate chains, could maintain appropriate CS and HS chain conformation, thereby increasing their accessibility [55].

C. Comparing unbinding force for SDC-1–VN and SD-4–VN complexes

All forces related to a single unbinding were gathered into histograms, formed separately for each retraction velocity. Figures 4(a) and 4(b) show exemplary histograms prepared for three distinct retraction speeds, i.e., 0.6, 6, and 19 μm/s, created for both types of molecular complexes. As typical for

TABLE II. The unbinding probability for syndecan-VN complexes, measured at various conditions: 50 m*M* TBS supplemented with 1 m*M* $CaCl_2$, 1 m*M* $MgCl_2$; PBS; 10 m*M* EDTA in PBS buffer; and in conditions of Mab-inhibited interaction. Unbinding probability is expressed as a mean ± standard deviation (SD).

Conditions	SDC-1–VN	SDC-4–VN
50 m*M* TBS supplemented with 1 m*M* $CaCl_2$, 1 m*M* $MgCl_2$	7.5% ± 0.6%	7.6% ± 0.8%
10 m*M* EDTA in PBS buffer	3.9% ± 0.4%	4.9% ± 0.3%
Mab-inhibited SDC-VN interaction	1.8% ± 0.3%	2.3% ± 0.2%

this type of measurement [29], the center and the unbinding event distribution width increase with the retraction velocity.

The observed asymmetry of histograms is a general feature of this type of measurement. The left tail of the histograms is limited by zero since the unbinding force cannot be negative. The right tail is theoretically unlimited but practically may include events unrelated to the unbinding of a single molecular complex. Some multiple ruptures [56] often constitute outliers, leading to increased mean unbinding force. The theoretical models do not consider this inherent asymmetry of the experimental results. Therefore, here, we decided to use the most probable unbinding force instead of the mean value. The most probable value in the lognormal distribution fit is not affected by the outliers, which can be considered an advantage of the lognormal distribution function over the Gaussian or other symmetrical functions. The use of the mode value is compatible with our previous works [5,26].

Knowing that a simple SMFS measurement of force curve does not deliver sufficient information on the nature of the intermolecular interaction, we applied dynamic force spectroscopy (DFS, [52]) to measure the most probable unbinding force, plotted as a function of the loading rate (describing how fast the applied force changes in time during molecular complex unbinding). In our experiments, retraction velocity varied from 0.1 to 19.0 μm/s, which corresponded to loading rates ranging from 540 to 380 000 pN/s. Then, we compared the obtained dynamic force spectra for both complexes [Fig. 4(c)]. The unbinding force for a single SCD-1–VN complex is smaller than the unbinding force for SCD-4–VN within the whole range of the applied loading rates. The proportionality quantified by linear regression shows a strong correlation

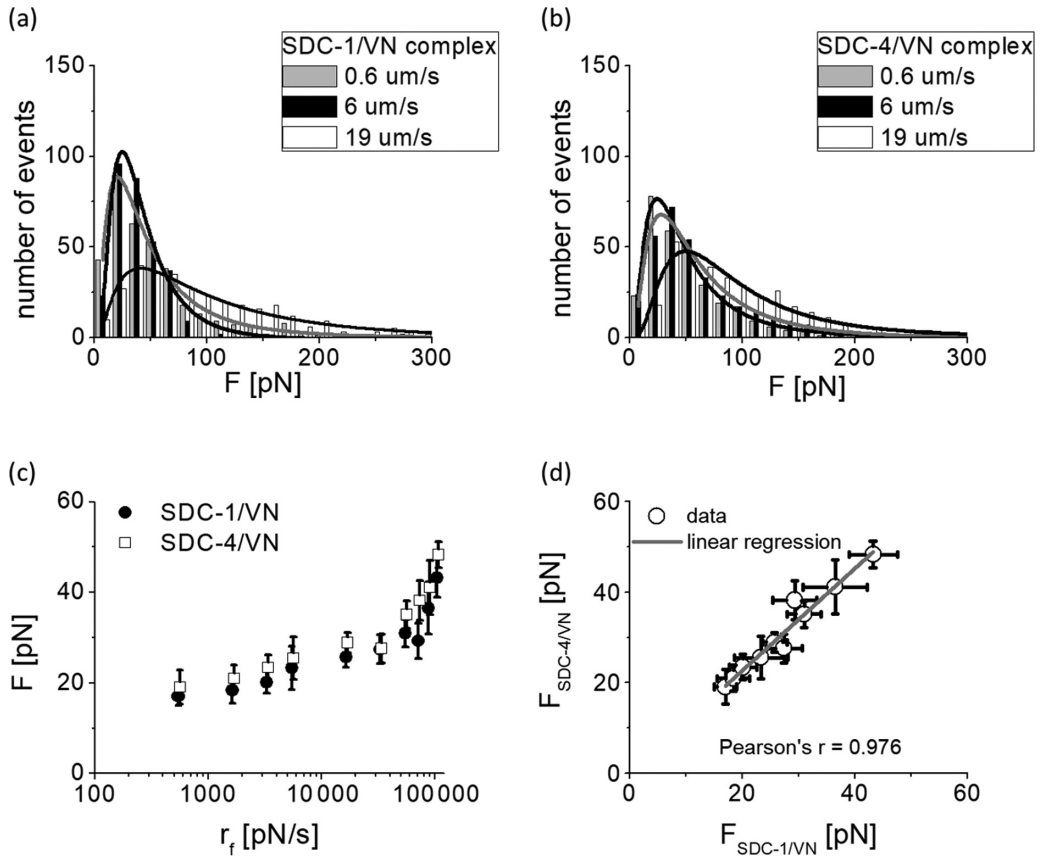

FIG. 4. (a), (b) Exemplary distributions of the unbinding events obtained for the unbinding of SDC-4–VN and SDC-1–VN ruptured at the retraction velocity of 0.6, 6, and 19 μm/s. Lines represent lognormal fits. (c) The unbinding force is plotted against the loading rate on a logarithmic scale (data represent mode and standard error, SE) (d) A correlation between the unbinding force for SDC-1–VN and SCD-4–VN complexes.

between the corresponding unbinding forces [$F_{\mathrm{SDC-4-VN}} = 1.13F_{\mathrm{SDC-1-VN}}$; Pearson's $r = 0.976$; see Fig. 4(d)]. We explain this relation by HS chain participation only in the binding with ECM proteins and attribute the observed small changes to structural differences in HS chains interacting with VN. CS chains in syndecan-1 are located closer to the cell membrane (Fig. 1). Thus, steric hindrance may prevent CS chains from reaching the HEP II binding site. Altogether, these results may indicate a conservativelike character of the binding site preserved for all syndecans in the interaction with ECM proteins.

D. Kinetic and thermodynamic parameters of SCD–VN complexes

In our study, the DFS spectra obtained for the unbinding of single SDC-1–VN complexes show two regions with shallow and steep slopes [Figs. 4(c) and 5]. The nonlinear character of the relation between the most probable unbinding force and the loading rate logarithm is similar to already reported data obtained for other biological complexes [29,42,57]. The nonlinear character of the F–$\ln(r_f)$ relation can be interpreted differently. It may denote a transition through an inner energy barrier that starts to dominate at high loading rates (BE, [54,57]), or it can be explained by an intrinsic feature of a single barrier, namely, its smooth shape and hence the force-induced shortening of the distance to the transition state (DHS, [38,58]). Therefore, to get deeper insights into the syndecan unbinding process from vitronectin, BE and DHS models were fitted to DFS spectra (Fig. 5).

The fits of BE and DHS models to the whole loading rate range resulted in $R^2_{\mathrm{adj}} < 0.9$. This value strongly suggests that the nonlinearity in the F–$\ln(r_f)$ relation originates from two, outer and inner, energy barriers. For the low loading rate range, from 540 to 34 000 pN/s (region I), the rupture forces increase almost linearly, indicating the presence of one, single dominant barrier. At higher loading rates, from 34 000 to 110 000 pN/s (region II), a steeper slope points to the presence of an inner energy barrier.

According to the BE model (and the DHS), two distinct slopes in the force spectrum correspond to the two kinetically distinct energy barriers. The linear region with shallow slope corresponds to the outer energy barrier [2.8 ± 0.3 pN; the goodness of the BE fit $R^2_{\mathrm{adj}} = 0.9554$, Fig. 3(a)]. The linear regression fitted for higher loading rates delivers the slope of 37.8 ± 1.1 pN ($R^2_{\mathrm{adj}} = 0.9986$), which translates into the kinetic parameters describing the passing over the inner energy barrier. The inner energy barrier only appears when the outer one is significantly lower due to force rupturing the molecular complex. Each energy barrier is characterized by its position in relation to the energy minimum and constant dissociation rate. These parameters for the SDC-1–VN complex obtained with the BE model were $x_\beta = 1.41 \pm 0.12$ nm, $k^0_{\mathrm{off}} = 0.69 \pm 0.42\ \mathrm{s}^{-1}$(the outer energy barrier dominating within the low loading rate regime) and $x_\beta = 0.111 \pm 0.003$ nm, $k^0_{\mathrm{off}} = 872 \pm 4\ \mathrm{s}^{-1}$ (the inner energy barrier dominating at larger loading rates). The BE model cannot be applied to determine the energy barrier height be-

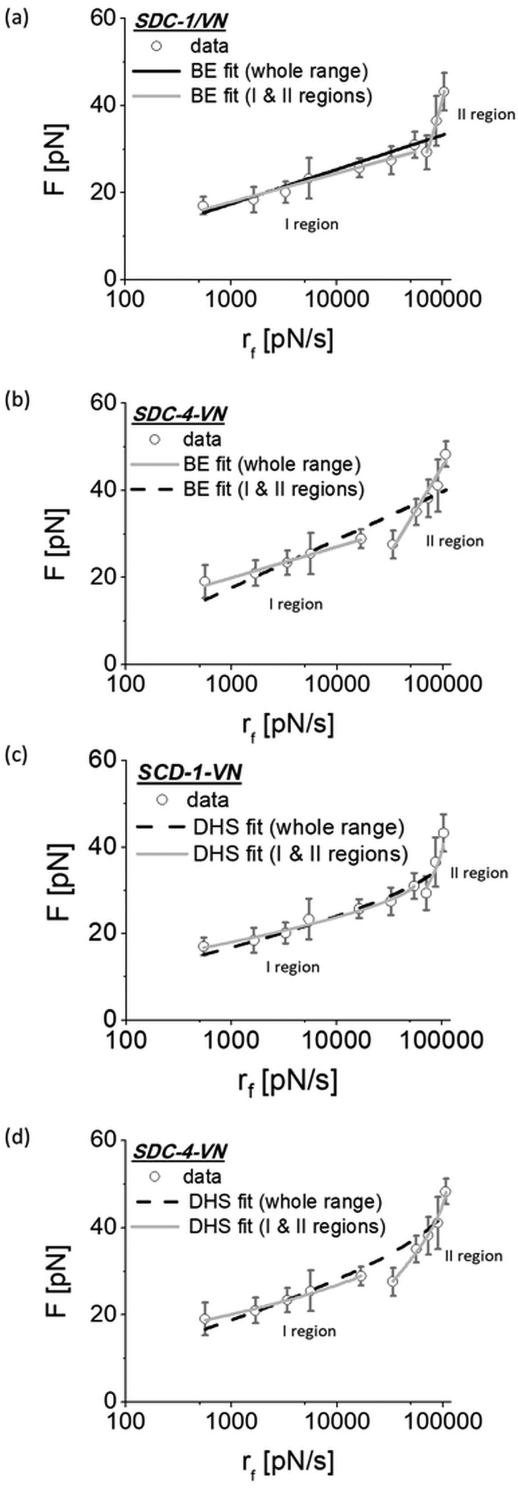

FIG. 5. The dynamic force spectrum obtained for the unbinding of SDC-VN complexes. Data (points) were fitted with both BE (a), (b) and DHS (c), (d) models. Dashed lines are the fits of BE and DHS models to the whole range of the loading rates, i.e., from 540 to 110 000 pN/s. The solid lines show the fits performed for low (from ~540 to 34 000 pN/s, region I) and high (34 000–110 000 pN/s, region II) loading rates. The error bars represent standard error (SE) multiplied by 2 (identical with the confidence level increase from 68% to 95%).

TABLE III. Thermodynamic and kinetic parameters describing the force-induced unbinding of two SDC-VN complexes.

Model	Loading rate range	x_β (nm)	$k^0_{\text{off}}(\text{s}^{-1})$	$\Delta G_\beta(k_BT)$	R^2_{adj}
		SDC-1–VN			
BE	540–34 000 pN/s	1.41 ± 0.12	0.69 ± 0.42	–	0.9554
	34 000–110 000 pN/s	0.111 ± 0.003	872 ± 4	–	0.9986
DHS	540–34 000 pN/s	2.86 ± 0.16	0.018 ± 0.011	14.6 ± 1.0	0.9815
	34 000–110 000 pN/s	0.439 ± 0.001	589 ± 156	3.0 ± 0.5	0.8598
		SDC-4–VN			
BE	540–34 000 pN/s	1.31 ± 0.10	0.51 ± 0.26	–	0.9789
	34 000–110 000 pN/s	0.23 ± 0.03	418 ± 56	–	0.9568
DHS	540–34 000 pN/s	2.65 ± 0.81	0.013 ± 0.035	14.2 ± 2.0	0.9868
	34 000–110 000 pN/s	0.53 ± 0.01	213 ± 19	4.2 ± 0.2	0.9900

cause all the information about the energy landscape shape is included in one parameter x_β. However, it is possible to calculate the height difference by applying the equation comparing dissociation rate constants:

$$|\Delta G_{b,\text{inner}} - \Delta G_{b,\text{outer}}| = -k_BT\,ln\left(k^{0,\text{inner}}_{\text{off}}/k^{0,\text{outer}}_{\text{off}}\right). \quad (5)$$

The obtained difference shows that the outer activation barrier is $\sim 7.14\,k_BT$ larger than the inner one.

The SDC-4 –VN complex rupture seems to proceed along the same pathways manifested in similar DFS spectra. Analogous BE-based analysis of the unbinding of the SCD-4 complex delivers a set of the kinetic parameters (i) $x_\beta = 1.31 \pm 0.10$ nm and $k^0_{\text{off}} = 0.51 \pm 0.26\,\text{s}^{-1}$ (the outer energy barrier, $R^2_{\text{adj}} = 0.9789$), and (ii) $x_\beta = 0.232 \pm 0.025$ nm and $k^0_{\text{off}} = 418 \pm 56\,\text{s}^{-1}$ (the inner energy barrier, $R^2_{\text{adj}} = 0.9568$). The BE-derived energy height difference is $\sim 6.71\,k_BT$, thus, relatively $0.5\,k_BT$ lower than for the SDC-1–VN complex.

In our earlier experiments, carried out for SDC-4 and VN, one linear region was observed due to the narrower loading rate range, i.e., between 10^4 and 10^5 pN/s [5]. The loading rate range for the SDC-VN interaction extended in the current study reveals two energy barriers characteristic of the unbinding force–ln(loading rate) relation. As compared to data already existing in the literature, the obtained results are different. The obtained x_β values were significantly larger than those reported for heparin [59] or SCD-4 [25] interaction with fibronectin. We relate the difference to the structure of heparin-binding sites in VN (encompassing amino acids in the protein sequence between positions 362 and 395, based on UniProt) and FN (52–272 and 1812–2082). Moreover, larger x_β indicates larger compliance of the molecular complex [60]. This agrees with our earlier results showing that the SDC-4–VN complex is softer than that formed by $\alpha_v\beta_5$-VN, and SDC-4–FN interaction is more compliant as compared to the $\alpha_5\beta_1$-VN one.

To validate the calculations of the energy difference between two barriers, simultaneously taking into account the shape of the energy landscape profile, the DHS model was fitted to the data for both complexes [Figs. 5(c) and 5(d)]. The fits of the DHS model to a whole range of the loading rates were characterized by $R^2_{\text{adj}} < 0.9$, which supported the hypothesis that the nonlinearity in the F–$\ln(r_f)$ relation originates in the presence of two, outer and inner, energy barriers. Thus, analogously as for the BE model, the DHS one was fitted to the same regions in the DFS spectra resulting in a set of the kinetic parameters. The advantage of this model is the direct determination of the energy barrier heights (Table III).

Kinetic parameters, obtained from the DHS model, derive the energy barrier height for both studied complexes. Their values were similar, i.e., $14.6 \pm 1.0\,k_BT$ and $14.2 \pm 2.0\,k_BT$ for the SCD-1–VN and SDC-4–VN complexes, respectively. The heights of the corresponding inner energy barriers were $3.0 \pm 0.5\,k_BT$ and $4.2 \pm 0.2\,k_BT$. However, for SCD-1–VN, the reliability of the received parameters is severely limited due to the fitting of only three experimental points in region II. Moreover, these three points do not exhibit significant curvature, and the curvature determines the ΔG_β parameter in the DHS model. Therefore, the value of ΔG_β for SCD-1–VN should be regarded as less reliable and significant than the results obtained for the parameters' uncertainty.

The difference between the energy barriers for SCD-4–VN is lower than for the SDC-1–VN complexes ($10.0\,k_BT$ versus $11.6\,k_BT$). In parallel, the lifetimes characterizing the crossing over the energy barriers for SDC-4–VN are higher, too. These results suggest that the force-induced unbinding of syndecan-1 from the HEP II binding site proceeds faster than the SDC-4–VN complex. The thermodynamic and kinetic parameters obtained from BE and DHS fits are summarized in Table III. They describe the force-induced unbinding of SDC-VN complexes. The fits were weighted with a standard error (SE). The fitting procedure involved multiple repetitions with different initial parameters to find an optimal set of parameters with sufficient convergence to experimental data. Usually, regardless of the starting values, the parameters converge to almost the same final values.

E. Rebinding during the unbinding of syndecan-VN complexes

To account for the rebinding, the FNDY model [39] was applied. This theoretical model considers (i) a near-equilibrium regime between the unbinding and rebinding of an individual complex, where the mean unbinding force is not dependent on the loading rate, and (ii) a kinetic regime where the unbinding force strongly depends on the loading rate. Due to nonsymmetric histograms of the unbinding force, in our analysis, we decided to use the most probable unbinding force instead of the mean value. The most probable value in the lognormal distribution fit is not affected by the outliers; thus, we minimize the presence of nontrue specific events. The rebinding affects the unbinding when force curves are collected at low

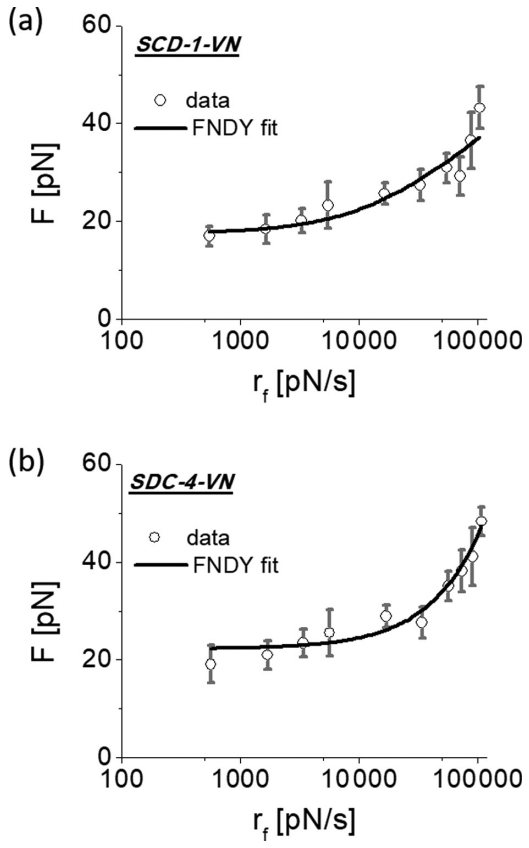

FIG. 6. Analysis of potential rebinding phenomenon based on the FNDY model. Data (points) were fitted with the FNDY model applied to the whole range of the loading rates (540–100 000 pN/s). The error bars represent standard error (SE) multiplied by 2 (the confidence level 95%).

loading rates (Fig. 6). The FNDY model divides the force spectrum into an equilibrium regime and a kinetic regime. In the former, the rebinding is possible (consequently x_β and k^0_{off} deviate from those obtained from the BE model for low loading rates), while in the latter it is negligible due to high rupture speed. The FNDY model fitted to the data matches DFS spectra for both studied complexes ($R^2_{\text{adj}} = 0.8851$ and $R^2_{\text{adj}} = 0.9374$, Table IV).

The transition from equilibrium to the kinetic regime is defined by the F_{eq} being 17.5 ± 1.4 pN and 22.2 ± 1.3 pN for SCD-1–VN and SDC-4–VN. In our experiments, such force values are recorded at the loading rates of 540 and 1700 pN/s. Thus, the results for the two first loading rates can be affected by the rebinding process. However, in the case of the SDC-4–VN complex, the FNDY fit (for the whole loading rate range) gives an unrealistically small value of x_β, suggesting that it is not rebinding but instead the outer barrier responsible for the F–$\ln(r_f)$ relation in the low loading rate range.

TABLE IV. Kinetics parameters for SDCs-VN complexes obtained based on the FNDY model.

	SDC-1–VN	SDC-4–VN
x_β (nm)	0.44 ± 0.22	$(9.7 \pm 1.8) \times 10^{-15}$
$k^0_{\text{off}@F_{\text{eq}}}$ (s^{-1})	843 ± 545	2397 ± 178
$\Delta G(k_BT)$	2.10 ± 0.40	3.80 ± 0.56
F_{eq} (pN)]	17.5 ± 1.4	22.2 ± 1.3
R^2_{adj}	0.8851	0.9374

V. CONCLUSIONS

The interaction of syndecans with ECM is based on mechanotransduction governing and regulating cell fate [61]. Specifically, syndecans are among the essential molecules for microbial infections and cancer development, although their presence and role is not fully understood in the integrin-mediated adhesion [13,62–64]. Here, we postulated that syndecan binding to HEP II binding sites involves only HS chains linked to the outermost part of the core syndecan protein. Therefore, we expect to obtain similar unbinding properties for both syndecans. The studied syndecans (SDC-1 and SDC-4) have appeared to be the Ca ion dependent molecules. Finally, we ask ourselves how kinetic and thermodynamic parameters are related to the structure and role of the syndecan-1 and syndecan-4 binding to the HEP II site in the vitronectin. From available structural data, at first sight, it seems that the interaction occurring between the syndecans and vitronectin involves mostly HS chains as they are the part that protrudes the most to the outside of the cell [1,22,23,61].

In our study, syndecan-1 and syndecan-4 interact with the same HEP II binding site of the vitronectin. Therefore, we expected that the binding-unbinding cycle would proceed similarly, regardless of the syndecan type. The syndecan interaction with vitronectin seems to rely mainly on HS chains being their most distant component, while the influence of the CS chains present in SDC-1 seems to be limited due to their membrane-proximal localization.

Thermodynamic and kinetic parameters from the force spectroscopy analysis for SDC-1 and SDC-4 complexes (Table III) indicate that unbinding properties are similar for both syndecan family members. Small variability in the thermodynamic and kinetics parameters (Table III) can stem from data analysis and may indicate weak structural alterations in the HS chains, possibly in chain sequence or sulfation pattern [65]. Overall, these data allow us to conclude that only HS chains participate in the interaction with ECM proteins which provides compliance to mechanical stress present in the cell microenvironment. In this way, HS chain affinity to ECM proteins may govern cancer invasion by altering the syndecans' ability to interact with cancer-related receptors present in the tumor microenvironment, thereby promoting the activation of various signaling cascades regulating tumor cell behavior.

ACKNOWLEDGMENTS

This work was supported by the National Science Centre (Poland) Project No. UMO-2014/15/B/ST4/04737 (M.L.). K.H. and A.P. acknowledge the Ministry of Science and Higher Education in Poland for financial support (Projects No. 0512/SBAD/2023 and Mo. 0512/SBAD/2120). The JPK purchase has been realized under the project cofounded by the Małopolska Regional Operational Program, Measure 5.1—Krakow Metropolitan Area as an important hub of the European Research Area for 2007–2013, Project No. MRPO.05.01.00-12-013/15.

[1] H. A. B. Multhaupt, A. Yoneda, J. R. Whiteford, E.-S. Oh, W. Lee, and J. R. Couchman, Syndecan signaling: When, where and why? J. Physiol. Pharmacol. **60**, 31 (2008).

[2] J. R. Bishop, M. Schuksz, and J. D. Esko, Heparan sulphate proteoglycans fine-tune mammalian physiology, Nature **446**, 1030 (2007).

[3] U. Lindahl and J.-p. Li, Chapter 3 Interactions between heparan sulfate and proteins—design and functional implications, Int. Rev. Cell Mol. Biol. **276**, 105 (2009).

[4] M. Bernfield, M. Gotte, P. W. Park, O. Reizes, M. L. Fitzgerald, J. Lincecum, and M. Zako, Functions of cell surface heparan sulfate proteoglycans, Annu. Rev. Biochem. **68**, 729 (1999).

[5] M. Lekka, K. Herman, J. Zemła, Ł. Bodek, G. Pyka-Fościak, D. Gil, J. Dulińska-Litewka, A. Ptak, and P. Laidler, Probing the recognition specificity of $\alpha_V\beta_1$ integrin and syndecan-4 using force spectroscopy, Micron **137**, 102888 (2020).

[6] C. Y. Fears and A. Woods, The role of syndecans in disease and wound healing, Matrix Biol. **25**, 443 (2006).

[7] C. W. Kim, O. A. Goldberger, R. L. Gallo, and M. Bernfield, Members of the syndecan family of heparan sulfate proteoglycans are expressed in distinct cell-, tissue-, and development-specific patterns, Mol. Biol. Cell **5**, 797 (1994).

[8] J. R. Couchman, Transmembrane signaling proteoglycans, Annu. Rev. Cell Dev. Biol. **26**, 89 (2010).

[9] M. Götte, A. M. Joussen, C. Klein, P. Andre, D. D. Wagner, M. T. Hinkes, B. Kirchhof, A. P. Adamis, and M. Bernfield, Role of syndecan-1 in leukocyte-endothelial interactions in the ocular vasculature, Invest. Ophthalmol. Visual Sci. **43**, 1135 (2002).

[10] M. Götte, Syndecans in inflammation, FASEB J. **17**, 575 (2003).

[11] M. D. Bass, M. R. Morgan, and M. J. Humphries, Integrins and syndecan-4 make distinct, but critical, contributions to adhesion contact formation, Soft Matter **3**, 372 (2007).

[12] V. F. Fiore, L. Ju, Y. Chen, C. Zhu, and T. H. Barker, Dynamic catch of a Thy-1-A5 B1 +syndecan-4 trimolecular complex, Nat. Commun. **5**, 4886 (2014).

[13] M. R. Morgan, M. J. Humphries, and M. D. Bass, Synergistic control of cell adhesion by integrins and syndecans, Nat. Rev. Mol. Cell Biol. **8**, 957 (2007).

[14] D. L. M. Beauvais and A. C. Rapraeger, Syndecan-1-mediated cell spreading requires signaling by $\alpha_V\beta_3$ Integrins in human breast carcinoma cells, Exp. Cell Res. **286**, 219 (2003).

[15] C. Mundhenke, K. Meyer, S. Drew, and A. Friedl, Heparan sulfate proteoglycans as regulators of fibroblast growth factor-2 receptor binding in breast carcinomas, Am. J. Pathol. **160**, 185 (2002).

[16] S. Saoncella, F. Echtermeyer, F. Denhez, J. K. Nowlen, D. F. Mosher, S. D. Robinson, R. O. Hynes, and P. F. Goetinck, Syndecan-4 signals cooperatively with integrins in a rho-dependent manner in the assembly of focal adhesions and actin stress fibers, Proc. Natl. Acad. Sci. USA **96**, 2805 (1999).

[17] S. Gopal, A. Bober, J. R. Whiteford, H. A. B. Multhaupt, A. Yoneda, and J. R. Couchman, Heparan sulfate chain valency controls syndecan-4 function in cell adhesion, J. Biol. Chem. **285**, 14247 (2010).

[18] M. A. Stepp, S. Pal-Ghosh, G. Tadvalkar, and A. Pajoohesh-Ganji, Syndecan-1 and its expanding list of contacts, Adv. Wound Care **4**, 235 (2015).

[19] I. C. Dews and K. R. MacKenzie, Transmembrane domains of the syndecan family of growth factor coreceptors display a hierarchy of homotypic and heterotypic interactions, Proc. Natl. Acad. Sci. USA **104**, 20782 (2007).

[20] J. R. Whiteford and J. R. Couchman, A conserved NXIP motif is required for cell adhesion properties of the syndecan-4 ectodomain, J. Biol. Chem. **281**, 32156 (2006).

[21] D. M. Beauvais, B. J. Ell, A. R. McWhorter, and A. C. Rapraeger, Syndecan-1 regulates $\alpha_V\beta_3$ and $\alpha_V\beta_5$ integrin activation during angiogenesis and is blocked by synstatin, a novel peptide inhibitor, J. Exp. Med. **206**, 691 (2009).

[22] E. R. Cruz-Chu, A. Malafeev, T. Pajarskas, I. V. Pivkin, and P. Koumoutsakos, Structure and response to flow of the glycocalyx layer, Biophys. J. **106**, 232 (2014).

[23] D. J. Carey, Syndecans: Multifunctional cell-surface co-receptors, Biochem. J. **327**, 1 (1997).

[24] D. L. M. Beauvais and A. C. Rapraeger, Syndecans in tumor cell adhesion and signaling, Reprod. Biol. Endocrinol. **2**, 3 (2004).

[25] T. M. Kennelly, Y. Li, Y. Cao, E. E. Qwarnstrom, and M. Geoghegan, Distinct binding interactions of $A_5\beta_1$-integrin and proteoglycans with fibronectin, Biophys. J. **117**, 688 (2019).

[26] K. Herman, M. Lekka, and A. Ptak, Unbinding kinetics of syndecans by single-molecule force spectroscopy, J. Phys. Chem. Lett. **9**, 1509 (2018).

[27] F. Burgos-Bravo, S. Martínez-Meza, A. F. G. Quest, C. A. M. Wilson, and L. Leyton, Application of force to a syndecan-4 containing complex with Thy-1–$A_V\beta_3$ integrin accelerates neurite retraction, Front. Mol. Biosci. **7**, 582257 (2020).

[28] K. Hozumi, K. Kobayashi, F. Katagiri, Y. Kikkawa, Y. Kadoya, and M. Nomizu, Syndecan- and integrin-binding peptides synergistically accelerate cell adhesion, FEBS Lett. **584**, 3381 (2010).

[29] M. Koehler, A. Fis, H. J. Gruber, and P. Hinterdorfer, AFM-based force spectroscopy guided by recognition imaging: A new mode for mapping and studying interaction sites at low lateral density, Methods Protoc. **2**, 6 (2019).

[30] D. J. Müller, J. Helenius, D. Alsteens, and Y. F. Dufrêne, Force probing surfaces of living cells to molecular resolution, Nat. Chem. Biol. **5**, 383 (2009).

[31] A. D. Gibson, J. A. Lamerdin, P. Zhuang, K. Baburaj, E. H. Serpersu, and C. B. Peterson, Orientation of heparin-binding sites in native vitronectin. Analyses of ligand binding to the primary glycosaminoglycan-binding site indicate that putative secondary sites are not functional, J. Biol. Chem. **274**, 6432 (1999).

[32] C. E. Wilkins-Port, R. D. Sanderson, E. Tominna-Sebald, and P. J. McKeown-Longo, Vitronectin's basic domain is a syndecan ligand which functions in trans to regulate vitronectin turnover, Cell Commun. Adhes. **10**, 85 (2003).

[33] K. Shin, B. C. Lechtenberg, L. M. Fujimoto, Y. Yao, S. S. Bartra, G. V. Plano, and F. M. Marassi, Structure of human vitronectin C-terminal domain and interaction with yersinia pestis outer membrane protein ail, Sci. Adv. **5**, eaax5068 (2019).

[34] J. E. Sader, I. Larson, P. Mulvaney, and L. R. White, Method for the calibration of atomic force microscope cantilevers, Rev. Sci. Instrum. **66**, 3789 (1995).

[35] D. A. Blake, P. Chakrabarti, M. Khosraviani, F. M. Hatcher, C. M. Westhoff, P. Goebel, D. E. Wylie, and R. C. Blake, Metal binding properties of a monoclonal antibody directed toward metal-chelate complexes, J. Biol. Chem. **271**, 27677 (1996).

[36] G. Bell, Models for the specific adhesion of cells to cells, Science **200**, 618 (1978).

[37] E. A. Evans and K. Ritchie, Strength of a weak bond connecting flexible polymer chains, Biophys. J. **76**, 2439 (1999).
[38] O. K. Dudko, G. Hummer, and A. Szabo, Intrinsic Rates and Activation Free Energies from Single-Molecule Pulling Experiments, Phys. Rev. Lett. **96**, 108101 (2006).
[39] R. W. Friddle, A. Noy, and J. J. De Yoreo, Interpreting the widespread nonlinear force spectra of intermolecular bonds, Proc. Natl. Acad. Sci. USA **109**, 13573 (2012).
[40] W. Hanley, O. McCarty, S. Jadhav, Y. Tseng, D. Wirtz, and K. Konstantopoulos, Single molecule characterization of P-selectin/ligand binding, J. Biol. Chem. **278**, 10556 (2003).
[41] G. Neuert, C. Albrecht, E. Pamir, and H. E. Gaub, Dynamic force spectroscopy of the digoxigenin-antibody complex, FEBS Lett. **580**, 505 (2006).
[42] E. P. Wojcikiewicz, M. H. Abdulreda, X. Zhang, and V. T. Moy, Force spectroscopy of LFA-1 and its ligands, ICAM-1 and ICAM-2, Biomacromolecules **7**, 3188 (2006).
[43] A. Taninaka, O. Takeuchi, and H. Shigekawa, Reconsideration of dynamic force spectroscopy analysis of streptavidin-biotin interactions, Int. J. Mol. Sci. **11**, 2134 (2010).
[44] A. M. Whited and P. S.-H. Park, Atomic force microscopy: A multifaceted tool to study membrane proteins and their interactions with ligands, Biochim. Biophys. Acta, Biomembr. **1838**, 56 (2014).
[45] F. T. Hane, S. J. Attwood, and Z. Leonenko, Comparison of three competing dynamic force spectroscopy models to study binding forces of Amyloid-β (1–42), Soft Matter **10**, 1924 (2014).
[46] A. Ptak, H. Gojzewski, M. Kappl, and H. J. Butt, Quantitative analysis of the interaction between an atomic force microscopy tip and a hydrophobic monolayer, J. Phys. Chem. C **114**, 21572 (2010).
[47] A. Ptak, H. Gojzewski, M. Kappl, and H. Butt, Influence of humidity on the nanoadhesion between a hydrophobic and a hydrophilic surface, Chem. Phys. Lett. **503**, 66 (2011).
[48] H. Gojzewski, M. Kappl, and A. Ptak, Effect of the chain length and temperature on the adhesive properties of alkanethiol self-assembled monolayers, Langmuir **33**, 11862 (2017).
[49] *Origin 8 User Guide* (OriginLab Corporation, Northampton, MA, 2007).
[50] F. Rico, L. Gonzalez, I. Casuso, M. Puig-Vidal, and S. Scheuring, High-speed force spectroscopy molecular dynamics simulations, Science **342**, 741 (2013).
[51] S. Allen, X. Chen, J. Davies, M. C. Davies, A. C. Dawkes, J. C. Edwards, C. J. Roberts, J. Sefton, S. J. B. Tendler, and P. M. Williams, Detection of antigen-antibody binding events with the atomic force microscope, Biochemistry **36**, 7457 (1997).
[52] K. Lebed, G. Pyka-Fosźciak, J. Raczkowska, M. Lekka, and J. Styczeń, Binding activity of patterned concanavalin a studied by atomic force microscopy, J. Phys.: Condens. Matter **17**, S1447 (2005).
[53] E. Evans, Looking inside molecular bonds at biological interfaces with dynamic force spectroscopy, Biophys. Chem. **82**, 83 (1999).
[54] R. Merkel, P. Nassoy, A. Leung, K. Ritchie, and E. Evans, Energy landscapes of receptor-ligand bonds explored with dynamic force spectroscopy, Nature **397**, 50 (1999).
[55] M. Kan, F. Wang, M. Kan, B. To, J. L. Gabriel, and W. L. McKeehan, Divalent cations and heparin/heparan sulfate cooperate to control assembly and activity of the fibroblast growth factor receptor complex, J. Biol. Chem. **271**, 26143 (1996).
[56] S. Getfert and P. Reimann, Hidden multiple bond effects in dynamic force spectroscopy, Biophys. J. **102**, 1184 (2012).
[57] F. Rico and V. T. Moy, Energy landscape roughness of the streptavidin-biotin interaction, J. Mol. Recognit. **20**, 495 (2007).
[58] B. Heymann and H. Grubmüller, Dynamic Force Spectroscopy of Molecular Adhesion Bonds, Phys. Rev. Lett. **84**, 6126 (2000).
[59] G. Mitchell, C. A. Lamontagne, R. Lebel, M. Grandbois, and F. Malouin, Single-molecule dynamic force spectroscopy of the fibronectin-heparin interaction, Biochem. Biophys. Res. Commun. **364**, 595 (2007).
[60] J. Liphardt, B. Onoa, S. B. Smith, I. Tinoco, Jr., and C. Bustamante, Reversible unfolding of single RNA molecules by mechanical force, Science **292**, 733 (2001).
[61] F. Gondelaud and S. Ricard-Blum, Structures and interactions of syndecans, FEBS J. **286**, 2994 (2019).
[62] B. Garcia, I. Fernandez-Vega, O. Garcia-Suarez, S. Castanon, and L. M. Quiros, The role of heparan sulfate proteoglycans in bacterial infections, J. Med. Microbiol. Diagn. **3**, 1000157 (2014).
[63] R. S. Aquino and P. W. Park, Glycosaminoglycans and Infection, Front. Biosci., Landmark Ed. **21**, 1260 (2016).
[64] D. Barbouri, N. Afratis, C. Gialeli, D. H. Vynios, A. D. Theocharis, and N. K. Karamanos, Syndecans as modulators and potential pharmacological targets in cancer progression, Front. Oncol. **4**, 4 (2014).
[65] K. Vuoriluoto, G. Högnäs, P. Meller, K. Lehti, and J. Ivaska, Syndecan-1 and -4 differentially regulate oncogenic K-ras dependent cell invasion into collagen through A2β1 integrin and MT1-MMP, Matrix Biol. **30**, 207 (2011).